Nested Fermi surfaces, optical peaks, and laser-induced structural transition in Al

S. J. Youn,[1,2] B. I. Min,[3] T. H. Rho,[1] and Kwang S. Kim[1,3]
[1]*National Creative Research Initiative Center for Superfunctional Materials and Department of Chemistry, Pohang University of Science and Technology, Pohang 790-784, Korea*
[2]*Department of Physics Education, Gyeongsang National University, Jinju 660-701, Korea*
[3]*Department of Physics, Pohang University of Science and Technology, Pohang 790-784, Korea*
(Received 22 September 2003; published 7 January 2004)

Electronic structure and optical properties of Al are reexplored by using the highly precise first-principles band method. The spin-orbit interaction, albeit small, plays a critical role in determining the topology of the Fermi surface and yields finite gap for interband transitions. The characteristic optical peaks in Al are shown to arise from the massive interband transitions between two parallel bands over the nested area of two Fermi surfaces. The laser-induced structural transition originates from this massive interband transition which causes the lattice softening via the excitation-driven charge transfer from the tetrahedral bonding to the octahedral antibonding sites.

DOI: 10.1103/PhysRevB.69.033101 PACS number(s): 71.18.+y, 64.70.Dv, 78.20.Bh, 78.20.Ci

Optical properties of Al have been studied for decades theoretically and experimentally.[1–10] Very recently, an interesting structural transition induced by the irradiation of 1.55 eV laser pulses has been reported.[11] It is expected that the transition occurs due to the band-structure collapse and the lattice instability caused by the strong interband electron excitation across a pair of parallel bands in Al. In fact, optical transitions with peaks at about 1.5 and 0.5 eV as well as the Fermi-surface properties are well described by the nearly free electron (NFE) model with two potential parameters and the effective mass.[1,12] However, the assignments for the interband transitions in terms of the band structure are not consistent among existing calculations. The 1.5-eV peak was assigned to the interband transitions at points near W point,[7] or at points on the Σ line.[8,10] In contrast, the 0.5 eV optical peak has received little attention. Lee and Chang[10] assigned 0.5-eV peak to the transitions at points near W on W-U-Δ plane.

In this Brief Report, we show that the transitions occur not only at specific **k** points on symmetry lines but massively in a wide **k**-space region determined by nested Fermi surfaces. Therefore the previous assignments correspond to only a part of massive transitions between two parallel bands occurring in a relatively wide **k** space. Further, based on the analysis of electronic states responsible for these massive interband transitions, we show explicitly that the laser-induced structural transition occurs due to weakening of bonding strength associated with the interband transitions.

Another closely related issue is the onset frequency of interband transitions. The onset frequency is usually assigned at the minimum frequency of σ_1 or ϵ_2, where σ_1 and ϵ_2 are the real part of the optical conductivity and the imaginary part of the dielectric constant, respectively. A zero gap for the interband transition was first suggested by Brust.[4] Szmulowicz and Segall[8] also obtained a zero gap, but they addressed the possibility of finite gap due to the spin-orbit interaction (SOI). However, Lee and Chang[10] obtained finite gap by using the pseudopotential method without the SOI. We have found that the inclusion of the SOI indeed gives rise to the finite interband gap. We also show that the SOI, albeit small, does play a critical role in determining the topology of the Fermi surfaces: the second and third Fermi surfaces are disconnected, once the SOI is taken into account.

We have investigated the electronic structure and the optical conductivity of Al by employing the highly precise first-principles local-density full-potential linearized augmented plane-wave (FLAPW) band method.[13] The SOI is included by the second variational method.[14] The Hedin-Lundqvist form for the exchange-correlation energy was employed in the local-density approximation (LDA). Interband contribution to the optical conductivity is obtained based on the formula derived from Kubo's linear response theory.[15] Each interband transition is broadened to simulate the lifetime broadening with width of 0.1 eV. Intraband Drude contribution is considered by taking parameters from experiments:[16] $\sigma(0)=3.23\times10^{17}$ sec^{-1}, $\tau=1.13\times10^{-14}$ sec. The FLAPW method is successfully applied to explore various optical properties of solids, such as optical conductivity, dielectric constant, magneto-optical Kerr effect, and magnetic circular dichroism.[17] The calculations are performed for fcc Al with the room-temperature experimental lattice constant of 4.049 Å,[18] since the optical properties are usually measured at room temperature.[16] We have used the cutoff energy of 14.44 Ry and muffin-tin radius of 2.6 a.u. for Al. The Fermi-level E_F and the self-consistent charge were obtained by using 2 992 special **k** points[19] in the irreducible part of Brillouin zone (IBZ) after a convergence test of E_F within 2.5 meV. Optical conductivity was calculated with a larger set of **k** points (419,220 points) in the IBZ in order to remove any error due to the insufficient number of **k** points.

Figure 1(a) presents energy band structure of Al along the symmetry lines. The bands from the NFE model are also given in comparison. Ashcroft's potential parameters were used in the NFE model calculation,[1] while the effective mass is set to 1.05 to fit the band width from the FLAPW calculation.[20] The effective mass does not affect the shape of the Fermi surface. Bandstructures from the FLAPW and the NFE model agree quite well around E_F. Since the NFE model is known to fit the experimental Fermi surfaces, our band structure should also give correct Fermi surfaces.[21] Below E_F, however, small deviations are found at the first band along X-W and along L-K. Deviation becomes significant at

 ©2004 The American Physical Society

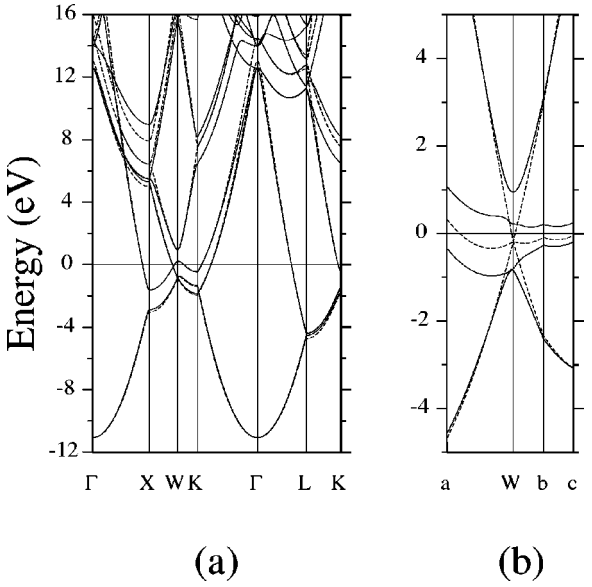

FIG. 1. Electronic energy band structure of Al. Energy bands by the FLAPW band method are shown in solid lines. For comparison, the energy bands by the NFE model and the free-electron model are shown in dashed lines in (a) and (b), respectively.

energies higher than 5 eV above E_F, indicating that the NFE model is valid only around E_F. Figure 1(b) will be explained later when discussing the Fermi surface in Fig. 3.

Figure 2 shows the optical conductivities both from our calculation and the experiment.[22] The solid line represents the calculated total optical conductivity which is the sum of the intraband Drude term and the interband contribution. Two characteristic peaks are seen at 0.38 eV and 1.44 eV in the interband contribution represented by the dotted line. The experimental peaks are found at 0.487 and 1.53 eV.[1,5] Hence the calculated peak positions are in good agreement with the experiment within error of 0.11 eV. Lower peak positions in the calculation would be attributed to the LDA, which underestimates the energy separation between occupied and unoccupied bands. The interband transition at 0.38 eV is difficult to be identified in total optical conductivity σ_1. However, as shown in the inset of Fig. 2, all the important transitions in Al can be found in the second derivative of the logarithm of σ_1. Negative peaks are recognized at 0.38 eV and 1.44 eV. The negative peak at 0 eV is due to the Drude intraband term.

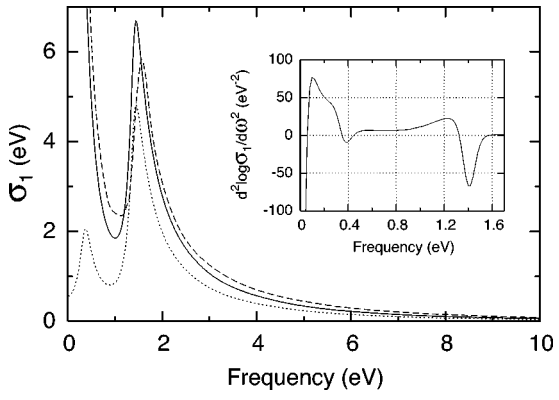

FIG. 2. Calculated optical conductivity of Al in comparison with the experiment[22] (dashed). The solid line represents the total optical conductivity including the intraband plus interband terms while the dotted line represents only the interband contribution. The inset shows $d^2 \ln \sigma_1 / d\omega^2$.

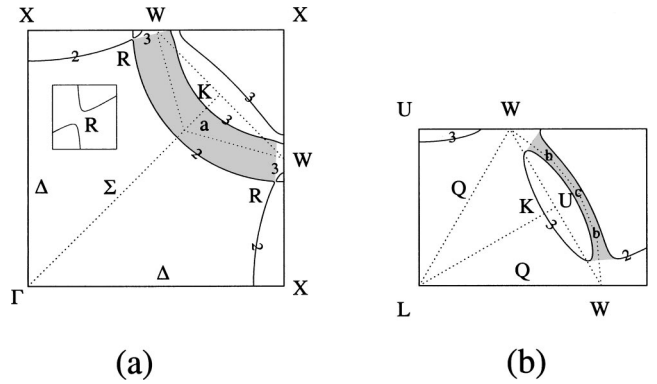

FIG. 3. Cross sections of the Fermi surface of Al around the K point in (a) (100) and (b) (111) planes. Numbers on lines represent band indices. Inset in (a) shows an expanded view (30×30) near the touching point R.

In Fig. 2, there are no structures at energies higher than 2 eV. This is contrary to previous calculations which show several steps.[8,10] Our result indicates that the steps are not intrinsic but artifacts resulting from the usage of insufficient number of **k** points for numerical integration of the matrix elements. The integration requires a large set of **k** points because the interband transitions occur only at limited regions in the reciprocal space and the matrix elements vary drastically. In addition, the Fermi level E_F should be obtained precisely since the shape of the Fermi surface depends sensitively on the value of E_F. Lee and Chang[10] obtained ϵ_2 with the artificial steps even though they used the largest set of **k** points among previous calculations (10 562 **k** points in the IBZ). Our result indicates that these artifacts can be avoided by using a larger set of **k** points (419 220 **k** points in the IBZ).

Figure 3 presents the Fermi surfaces where the SOI is explicitly taken into account. There are three pieces of the Fermi surfaces: the second zone hole Fermi surface around Γ, the third zone electron arm Fermi surface around K, and a small electron Fermi surface near W. The arm Fermi surface is a part of the toroidal Fermi surface around X in the square face of the BZ. The small Fermi surface near W is not an independent Fermi surface but a part of the third zone Fermi surface due to the inversion symmetry with respect to W on the X-W-X line. Thus, the Fermi surface consists of two parts: a large hole Fermi surface around Γ and a toroidal Fermi surface in the square face.

As mentioned above, there is a controversy about the connectivity of two Fermi surfaces near W. Ashcroft[1] proposed disconnected Fermi surfaces by fitting experimental Fermi surfaces using the NFE model. But he mentioned a possibility of a connected Fermi surface based on magnetoresistance measurement. However, a connected Fermi surface was proposed in the other NFE model calculation[4] and also by using

the APW calculation.[8] A connected Fermi surface implies that there is only a large single sheet of Fermi surface and that there is no gap for the interband transition between the second and third bands. In addition, a giant orbit can be formed in the (100) plane by the second zone Fermi surface bridged by the small third zone Fermi surface.

We have obtained a connected Fermi surface when the SOI is not included. However, when the SOI is taken into account, two Fermi surfaces are separated as shown in the inset of Fig. 3(a). The inset is an enlarged view of the Fermi surface around R point by 30×30, where R is the expected point for the Fermi surface touching. Accordingly the possibility of the giant circle in the (100) plane is ruled out. The minimum gap between the second and the third bands is $\sim$11 meV at $\mathbf{k}=(0.410,0.967,0)$. Hereafter, reciprocal vectors $\mathbf{G}$ are given in unit of $(2\pi/a)$, where a is the lattice constant of Al. Since this gap is smaller than the room temperature (25 meV), the Fermi surface should be measured at low temperature. Note that, due to the lifetime broadening, the calculated interband contribution in Fig. 2 has finite value at zero frequency. The above discussion reflects that the SOI, in spite of its small magnitude, plays a critical role in determining the topology of the Fermi surface and the interband gap of Al.

In Fig. 3(a), one can notice that the two Fermi surfaces are nested in the (110) direction between the second and third zone Fermi surfaces. Fermi-surface nesting is induced by a constant crystal field $2|V_{200}|$ which lifts the degeneracy between the second and third bands in the (100) plane of the reciprocal space. Here V_{200} is the Fourier coefficient of the crystal potential at $\mathbf{G}=(200)$. In the shaded region between two nested Fermi surfaces, the second and third bands are parallel with a band splitting of $2|V_{200}|$. Using the NFE model, Ashcroft estimated $2|V_{200}|=1.53$ eV which corresponds to the optical peak position at 1.53 eV. Furthermore, there are other nested Fermi surfaces in the (111) plane arising from the second and third zone Fermi surfaces [Fig. 3(b)]. Here the Fermi-surface nesting is induced by a constant crystal field $2|V_{111}|$ which is related to the 0.487-eV optical peak.

Figure 1(b) shows energy bands along certain lines inside the shaded regions of Figs. 3(a) and 3(b). The FLAPW band is compared with the free-electron (FE) band. The second and third bands are degenerate near E_F in the FE band. Two degenerate bands result from two wave vectors of (111) and $(11\bar{1})$ at the a point and from (000) and (111) at the c point, respectively. These degenerate bands are split by the crystal field. One can estimate the splittings from the NFE model to be $2|V_{002}|\sim1.5$ eV and $2|V_{111}|\sim0.5$ eV at the a and c points, respectively, which agree well with the calculated peak positions at 1.44 and 0.38 eV.

Previous investigations[2,7,8,10] on the interband transitions along Γ-K or Γ-W lines give only partial information on the massive interband transitions occurring in the shaded region of Fig. 3(a). Also the characteristic peak at 0.38 eV in the calculation arises from the massive interband transitions occurring in the shaded region of Fig. 3(b). In order to see the parallel band effect explicitly, we plot in Fig. 4 the momentum component of the oscillator strength, $\sigma(\mathbf{k},\omega)$, along the lines in Fig. 1. Integration of $\sigma(\mathbf{k},\omega)$ over $\mathbf{k}$ gives the optical conductivity $\sigma(\omega)$. As seen in Fig. 4(a), if $\sigma(\mathbf{k},\omega)$ is plotted along the symmetry lines, strong transitions take place only at small regions around W and K, which is not enough to yield two characteristic peaks. Figure 4(b), however, clearly shows that the massive interband transitions take places in the nested area. The interband transitions near a yield the 1.44-eV peak in $\sigma(\omega)$, while the transitions near c yield the 0.38-eV peak. Thus, the characteristic peaks in $\sigma(\omega)$ arise from the massive interband optical transitions between two parallel bands over the nested area of two Fermi surfaces.

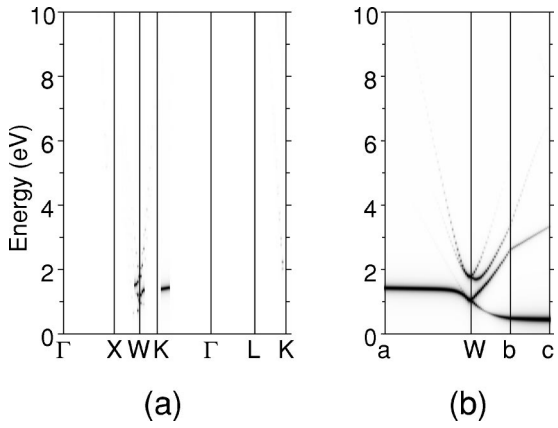

FIG. 4. Momentum component of the oscillator strength, $\sigma(\mathbf{k},\omega)$, along the lines in Fig. 1.

The structural transition induced by laser of 1.55 eV energy[11] can be ascribed to these massive interband transitions occurring inside the nested area of two Fermi surfaces. In order to see the effect of 1.55-eV transition, we have plotted in Fig. 5 the charge-density distributions in (110) plane for the second (below E_F) and third (above E_F) bands at the point a. Interestingly, two bands give very different interstitial charge distributions. As shown in Fig. 5(a), the second band has bonding character with interstitial electrons at the tetrahedral sites, whereby four surrounding Al atoms are strongly bound. In contrast, the third band has an anti-

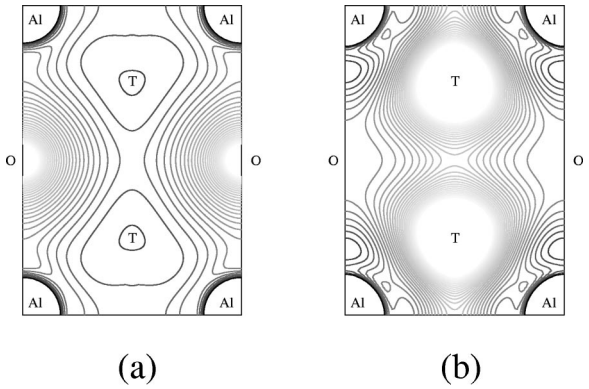

FIG. 5. Partial charge density for (a) the second and (b) third bands in (110) plane. Core charges are not plotted. Darkness is proportional to the charge density. T and O represent the tetrahedral and octahedral sites, respectively.

bonding character with high charge density between Al and the octahedral site, as shown in Fig. 5(b). Therefore, once the electrons are excited from the second band to the third band, the bonding strength between Al atoms becomes weak and accordingly the structural phase transition occurs through lattice softening.

In conclusion, we have calculated the optical conductivity σ_1 of Al very precisely by using a huge number of **k** points and by including the SOI explicitly in the calculation. The SOI plays a critical role in determining the topology of the Fermi surface and gives finite interband gap. The characteristic optical peaks at 0.5 and 1.5 eV are identified as the interband transitions occurring between two parallel bands over the nested area of two Fermi surfaces. The origin of the structural phase transition induced by intense laser pulses of 1.55 eV is shown to be the massive interband transitions inside the nested Fermi surfaces, which soften lattice by transferring charge from the tetrahedral bonding to the octahedral antibonding sites.

This work was supported by KISTEP/CRI of Korean ministry of Science and Technology. B.I.M. acknowledges the support by the KOSEF through the eSSC at POSTECH.

[1] N.W. Ashcroft, Philos. Mag. **8**, 2055 (1963).
[2] H. Ehrenreich, H.R. Philipp, and B. Segall, Phys. Rev. **132**, 1918 (1963).
[3] W.A. Harrison, Phys. Rev. **147**, 467 (1966).
[4] D. Brust, Phys. Rev. B **2**, 818 (1970).
[5] L.W. Bos and D.W. Lynch, Phys. Rev. Lett. **25**, 156 (1970).
[6] E. Shiles, T. Sasaki, M. Inokuti, and D.Y. Smith, Phys. Rev. B **22**, 1612 (1980), and references there in.
[7] J. Callaway and D.G. Laurent, Phys. Lett. **84A**, 499 (1981).
[8] F. Szmulowicz and B. Segall, Phys. Rev. B **24**, 892 (1981).
[9] E.G. Maksimov, I.I. Mazin, S.N. Rashkeev, and Y.A. Uspenski, J. Phys. F: Met. Phys. **18**, 833 (1988).
[10] K.-H. Lee and K.J. Chang, Phys. Rev. B **49**, 2362 (1994).
[11] C. Guo, G. Rodriguez, A. Lobad, and A.J. Taylor, Phys. Rev. Lett. **84**, 4493 (2000).
[12] N.W. Ashcroft and N.D. Mermin, *Solid State Physics* (Sounders Co., Philadelphia, 1976).
[13] E. Wimmer, H. Krakauer, M. Weinert, and A.J. Freeman, Phys. Rev. B **24**, 864 (1981); M. Weinert, E. Wimmer, and A.J. Freeman, *ibid.* **26**, 4571 (1982).
[14] A.H. MacDonald, W.E. Pickett, and D.D. Koelling, J. Phys. C **13**, 2675 (1980); S.J. Youn, W. Mannstadt, and A.J. Freeman, J. Comput. Phys. **172**, 387 (2001).
[15] C.S. Wang and J. Callaway, Phys. Rev. B **9**, 4897 (1974).
[16] D.Y. Smith and B. Segall, Phys. Rev. B **34**, 5191 (1986).
[17] S.J. Youn, B.I. Min, and A.J. Freeman, Phys. Rev. B **66**, 052512 (2002); R. Asahi, Y. Taga, W. Mannstadt, and A.J. Freeman, *ibid.* **61**, 7459 (2000); R. Asahi, W. Mannstadt, and A.J. Freeman, *ibid.* **59**, 7486 (1999); M. Kim, A.J. Freeman, and R. Wu, *ibid.* **59**, 9432 (1999); R. Wu, D. Wang, and A.J. Freeman, Phys. Rev. Lett. **71**, 3581 (1993).
[18] H.M. Otte, W.G. Montague, and D.O. Welch, J. Appl. Phys. **34**, 3149 (1963).
[19] H.J. Monkhorst and J.D. Pack, Phys. Rev. B **13**, 5188 (1976).
[20] Occupied bandwidth is 11.07 eV for the FLAPW calculation, while the free electron value is 11.66 eV.
[21] The area of the inner ring ξ of third zone Fermi surface in (100) plane is found to be 86.9×10^6 G which is in good agreement with experimental value of 88. 8×10^6. If a smaller lattice constant of 4.02 Å at low temperature is used, the area becomes 88.2×10^6 which shows a better agreement. See J.R. Anderson and S.S. Lane, Phys. Rev. B **2**, 298 (1970).
[22] D.Y. Smith, E. Shiles, and M. Inokuti, in *Handbook of Optical Constants of Solids*, edited by E.D. Palik (Academic, Orlando, 1985).